Kinematic Analysis of SCARA Robots

Sijia Peng, Teng Hu*

School of Mechatronic Engineering, Southwest Petroleum University, Chengdu 610500, China

* Corresponding author

Abstract: The SCARA robot, formally known as the Selective Compliance Assembly Robot Arm (SCARA), is characterized by its high speed and precise positioning capabilities. These advantages have led to its widespread adoption in applications such as assembly, material handling, and grasping. Consequently, SCARA robots contribute significantly to improving production efficiency and have attracted substantial research interest within the academic community. Due to its inherent structural configuration, the SCARA robot typically features a bulky base and certain link members. This volumetric characteristic poses challenges for deployment in workspaces with strict size constraints. To enhance the applicability of SCARA robots in such specific scenarios, this study focuses on modeling an optimized structural variant. The model is developed based on the robot's architecture: its workspace is analyzed, a schematic diagram and corresponding Denavit-Hartenberg (DH) parameters are established, and a kinematic model is constructed within MATLAB along with the associated reference frames. The homogeneous transformation method is employed to formulate the SCARA robot's kinematic model. Subsequently, the closed-form solutions for both the forward and inverse kinematics are derived. This comprehensive kinematic analysis provides a foundational reference for research into SCARA robot control methodologies.

Keywords: SCARA robot; Kinematic Solutions; MATLAB.

1. Introduction

Substation operation and maintenance requirements, particularly concerning safety performance, are becoming increasingly stringent. Transformers operate continuously under persistent electrical loads, where a failure in their insulation system can lead to significant economic losses. Currently, the primary method for detecting potential transformer faults relies on periodic oil sampling – extracting and analyzing the insulating liquid within the unit. However, this manual sampling approach presents significant drawbacks: it is resource-intensive both financially and laborwise. Critically, conducting sampling on a transformer experiencing an incipient fault or malfunction poses substantial safety hazards for personnel involved [1].

To enhance personnel safety and facilitate effective transformer insulating oil sampling, a SCARA robot is employed for automated oil extraction. During operation, the robot's end-effector is specifically designed with passive compliance, mitigating stringent requirements on the robot's motion accuracy and trajectory tracking [2-3]. Furthermore, the SCARA (Selective Compliance Assembly Robot Arm) configuration offers inherent advantages, including a simple mechanical structure, high operational speed, and exceptional positioning precision [4]. Consequently, utilizing the SCARA robot for oil sampling tasks provides superior cost-effectiveness compared to deploying a six-degree-of-freedom (6-DoF) robotic manipulator.

The confined workspace inherent to the oil extraction task presents a significant constraint. Standard SCARA robots, often characterized by relatively large physical dimensions, prove unsuitable under these spatial limitations [5-6]. To accomplish the work within this specific operating environment, a custom-designed SCARA robot with an appropriately compact size was developed. Based on the kinematic structure of this customized SCARA robot, its Denavit-Hartenberg (DH) parameters were formally derived. Subsequently, a kinematic model was rigorously constructed

within the MATLAB environment, enabling detailed workspace analysis. Using homogeneous transformation matrices, the forward and inverse kinematic equations for this structurally optimized SCARA robot were explicitly formulated. These derived kinematic models provide a critical technical reference for implementing effective motion control strategies for SCARA robots with this specific customized architecture.

2. SCARA Robot Structure and Modeling

The structural configuration of the SCARA robot investigated in this study is depicted in Fig. 1. comprises three revolute joints (J1, J2, J3) and one prismatic joint (J0). The designated link lengths are as follows: Shoulder Joint (Link 0) length $L_0 = 120$ mm, Elbow Joint (Link 1) length $L_1 = 220$ mm, and Wrist Joint (Link 2) length $L_2 = 200$ mm. The prismatic joint J0 exhibits a translational range of 0-40 mm, while the revolute joints operate within the following rotational ranges: J1 rotates within [-90°, +90°], J2 within [-164°, +164°], and J3 provides continuous rotation capability with a full [-360°, +360°] range. The rotational angles of all robot joints are currently at 0°. The vertical displacement of joint J0 is 0. The base coordinate system is positioned flush with the top surface of link L0 and centered on the base. The coordinate system at joint J1 is located on the top surface of link L0 and coincides with the rotational center of joint J1. The coordinate system at joint J2 resides on the top surface of link L1 and aligns with the rotational center of joint J2. The coordinate system at joint J3 is fixed to the top surface of link L2 and centered on the rotational axis of joint J3. The endeffector coordinate system is rigidly affixed to the bottom surface of link L2 at the rotational center of joint J3.

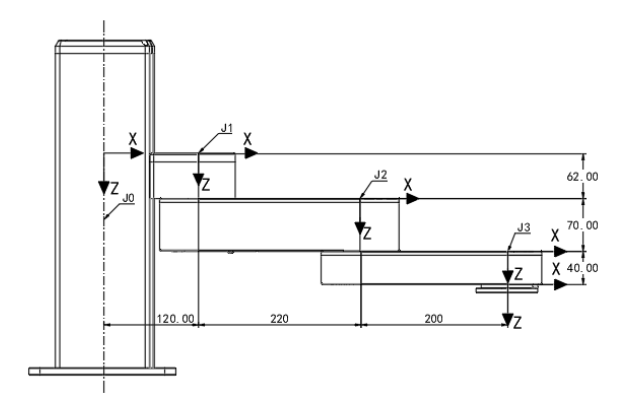


Figure .1 SCARA Robot Structural Diagram

Derived from the manipulator kinematics, the standard Denavit-Hartenberg (DH) parameters for the robot are tabulated in Table 1.

Table 1. DH Parameters of SCARA Robot

	a	alpha	d	theta
L0	120	0		0
L1	220	0	62	0
L2	200	0	70	0
L3	0	0	40	0

Implementing these DH parameters within the MATLAB environment using the conventional DH modeling approach [7], while incorporating joint motion constraints, yields the simulated kinematic model of the SCARA robot is illustrated in the Fig.2

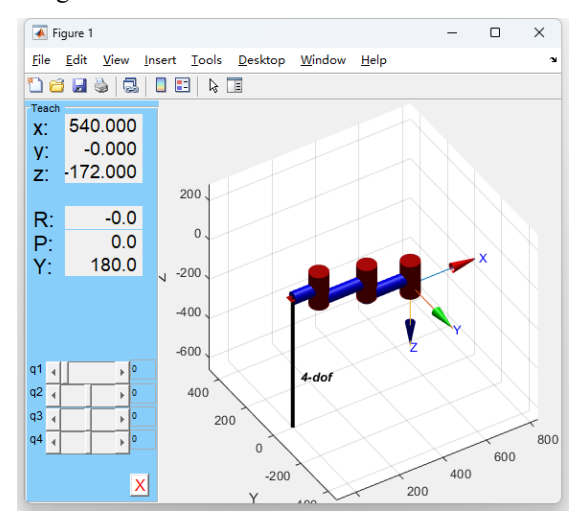


Figure .2 Kinematic Modeling of SCARA Robots

Computational modeling in MATLAB enables derivation of transformation matrices and corresponding manipulator poses during subsequent SCARA kinematic analysis, thus verifying the correctness of the inverse kinematic equations.

3. SCARA Robot Workspace Analysis

Primary methodologies for robotic workspace analysis include direct geometric boundary examination, Monte Carlo-based random sampling of joint configurations, By analyzing the DH parameters of the SCARA robot [8-10]. Geometric boundary methods and Monte Carlo sampling demonstrate efficacy for low-degree-of-freedom (DOF) manipulators, while Jacobian-based boundary surface analysis offers enhanced precision at the expense of significant computational complexity. Given the intrinsically

simple kinematic structure of the SCARA robot investigated in this study, its workspace can be rapidly characterized through geometric boundary construction augmented by Monte Carlo simulation.

The XOY-plane projection of the SCARA robot's workspace is illustrated in Fig.3. Joint limit configurations occur under two critical conditions: when the elbow joint angle (J2) equals -90° with concurrent wrist joint angle (J3) at -164°, or when J2 = 90° with J3 = 164°. Workspace boundary determination proceeds through three parametric analyses: (1) With the wrist joint fixed at $\pm 164^\circ$, elbow joint rotation traces the internal circular-arc boundary; (2) With the wrist joint locked at 0°, elbow joint motion generates the *major external circular-arc boundary*; (3) With the elbow joint constrained to $\pm 90^\circ$, wrist joint rotation establishes the *minor external circular-arc boundary*.

In SCARA robot modeling, the links can be approximated as rigid links. The achievable workspace of the SCARA manipulator within the XY-plane can be initially determined based on its link lengths and joint limit constraints. However, accounting for the physical link dimensions reveals that the maximum rotational range of the elbow joint (J2) is limited to 120°. Consequently, the effective workspace requires calibration to accurately reflect operational boundaries.

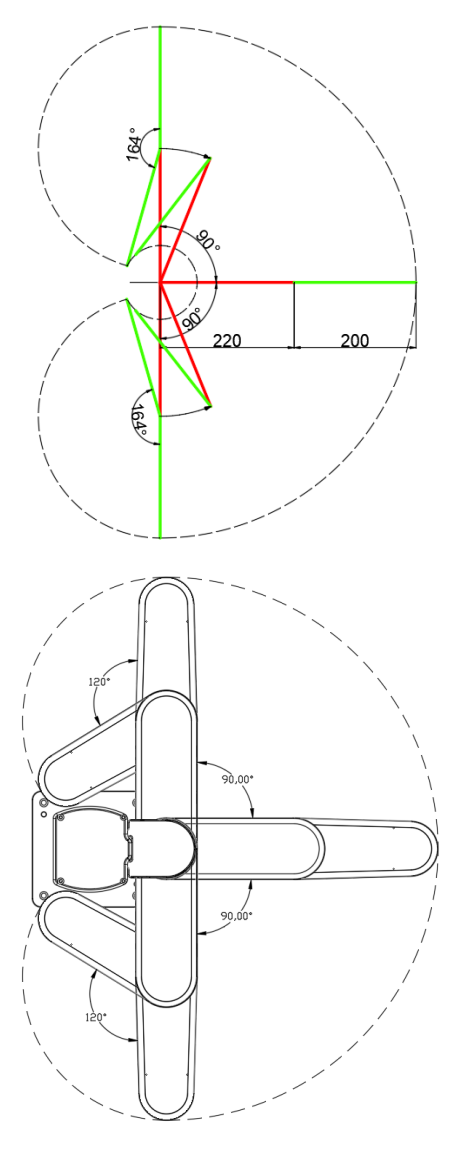


Figure .3 Workspace of SCARA Robot

When the size of each link of the SCARA robot is not

considered. Take advantage of the projection on this XOY plane, the complete three-dimensional workspace of the SCARA robot is generated through translational displacement along the vertical axis within the operational range of the shoulder joint (J0).

The workspace was validated using the Monte Carlo method through randomized sampling of joint configurations within their operational ranges. With a sample size of N=60,000, the resulting SCARA robot workspace is illustrated in Fig. 4.

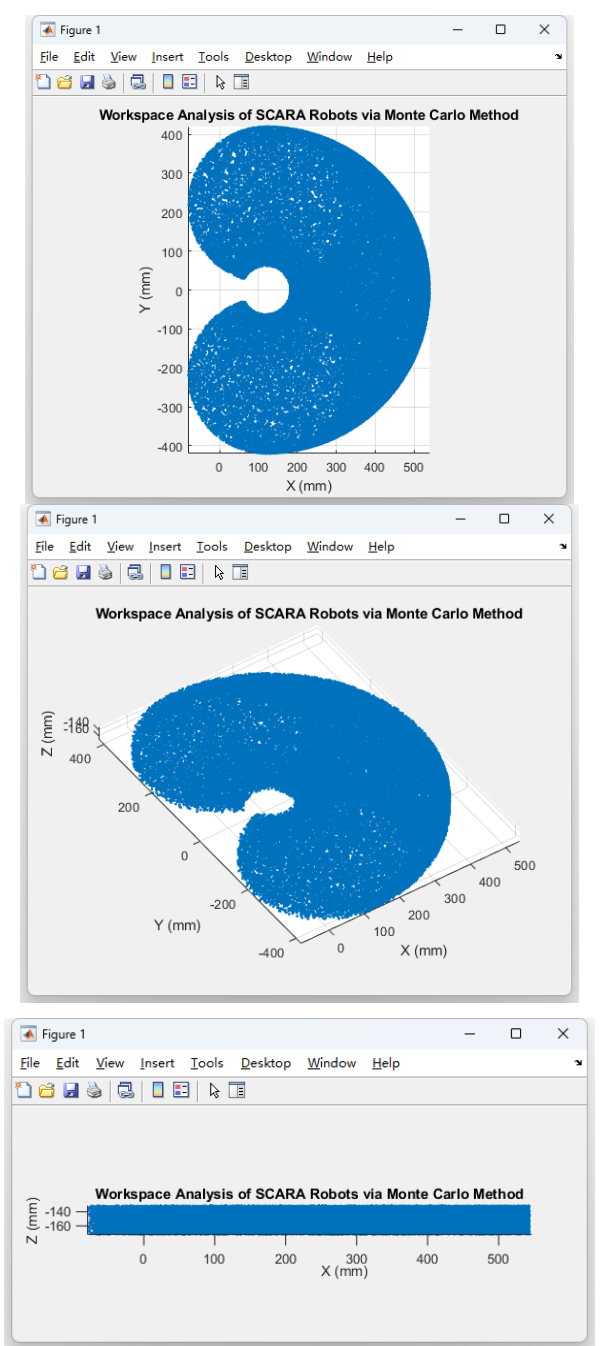


Figure.4 Workspace Determination via Monte Carlo Method

Considering the size of the connecting rods of each joint of the SCARA robot, when the joints of the SCARA robot are in the limit position, the size of the base of the SCARA robot will limit the maximum angle of rotation of its joints, and the projection of the base of the SCARA robot in the XOY plane is shown in Figure 5.

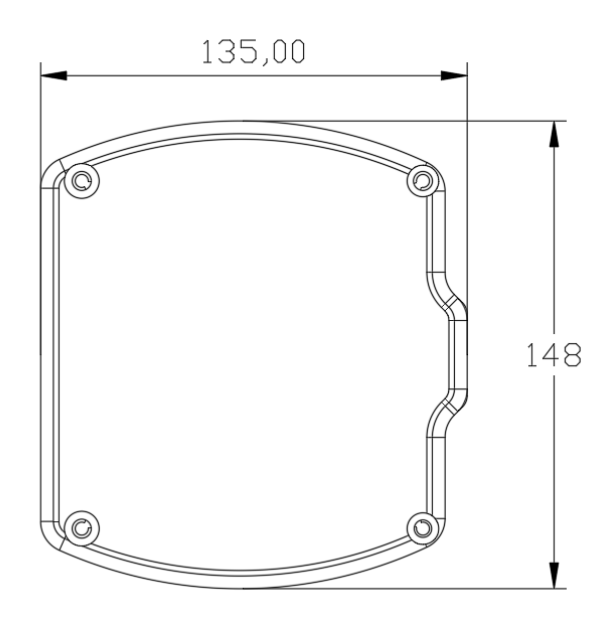


Figure.5 SCARA Robot Base Dimensions

The actual workspace projection of the SCARA robot onto the XOY plane, with the exclusion volume of the base structure, is depicted in Fig. 6.

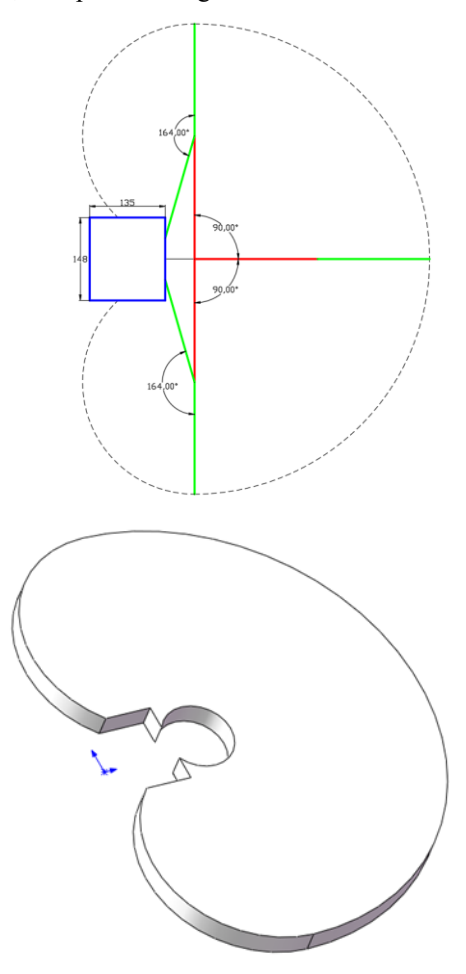


Figure.6 SCARA robot workspace calibration

4. SCARA Robot Kinematics Analysis

The predominant methodologies for characterizing endeffector pose relative to the robot base frame are the homogeneous transformation method and screw theory. The homogeneous transformation approach offers computational efficiency by representing rigid-body position and orientation within a unified 4×4 matrix framework. Conversely, screw theory utilizes screw coordinates to describe joint motion, providing clear geometric interpretation while exhibiting singularity-free properties[11-12]. Given the relatively simple kinematic structure of the SCARA robot investigated in this study, the homogeneous transformation method was selected for pose description.

4.1. SCARA Robot Forward Kinematics

Deriving the end-effector pose matrix in Cartesian space homogeneous requires establishing successive transformations between consecutive coordinate frames, where each frame $\{i\}$ is defined relative to its predecessor $\{i$ -1); cascading these individual transformations yields the composite position and orientation of the terminal frame {4} with respect to the base frame $\{0\}$.

The transformation defining frame {i} relative to its predecessor frame {i-1} is geometrically interpreted as a sequence of elementary operations: rotation about one principal axis (x, y, or z) of frame {i-1} followed by translation along the coordinate axes of that same frame. Kinematic analysis of this SCARA manipulator specifically reveals that frame {1} is derived from the base frame {0} through a 180° rotation about the x-axis coupled with an 80 mm translation along the x-axis, constituting the homogeneous transformation matrix as follows:

$${}^{4}T = \begin{bmatrix} \cos(\theta_{1} + \theta_{2} + \theta_{3}) & -\sin(\theta_{1} + \theta_{2} + \theta_{3}) & 0 & 120 + 220\cos(\theta_{1}) + 200\cos(\theta_{1} + \theta_{2}) \\ \sin(\theta_{1} + \theta_{2} + \theta_{3}) & \cos(\theta_{1} + \theta_{2} + \theta_{3}) & 0 & 220\sin(\theta_{1}) + 200\sin(\theta_{1} + \theta_{2}) \\ 0 & 0 & 1 & z_{0} + 172 \\ 0 & 0 & 0 & 1 \end{bmatrix}$$

4.2. SCARA Robot Inverse Kinematics

Given the end-effector transformation matrix T for the SCARA robot, inverse kinematics analysis is performed to derive the corresponding joint angles. Established approaches include numerical and geometric solution methods [14-15]. Numerical techniques encompass algorithms such as Particle Swarm Optimization [16], Sine Cosine Algorithm [17], and Genetic Algorithms [18]. Compared to geometric methods, numerical approaches demonstrate superior generality for high-degree-of-freedom or kinematically manipulators, operating without geometric constraints.

$${}_{0}^{4}T = \begin{bmatrix} \cos(\alpha + \beta + \gamma) & -\sin(\alpha + \beta + \gamma) & 0 & 120 + 220\cos(\alpha) + 200\cos(\alpha + \beta) \\ \sin(\alpha + \beta + \gamma) & \cos(\alpha + \beta + \gamma) & 0 & 220\sin(\alpha) + 200\sin(\alpha + \beta) \\ 0 & 0 & 1 & z_{0} + 172 \\ 0 & 0 & 0 & 1 \end{bmatrix}$$

With all elements of the end-effector transformation matrix being known quantities, the inverse transformation matrix for the first joint (J1) can be computationally derived as follows:

$${}_{0}^{1}T = \begin{bmatrix} 1 & 0 & 0 & 120 \\ 0 & 1 & 0 & 0 \\ 0 & 0 & 1 & z_{0} \\ 0 & 0 & 0 & 1 \end{bmatrix}$$
 1

the Consequently, homogeneous transformation matrices are derived as follows:

$${}^{2}_{1}T = \begin{bmatrix} \cos(\theta_{1}) & -\sin(\theta_{1}) & 0 & 220\cos(\theta_{1}) \\ \sin(\theta_{1}) & \cos(\theta_{1}) & 0 & 220\sin(\theta_{1}) \\ 0 & 0 & 1 & 62 \\ 0 & 0 & 0 & 1 \end{bmatrix}$$

$${}^{3}_{2}T = \begin{bmatrix} \cos(\theta_{2}) & -\sin(\theta_{2}) & 0 & 200\cos(\theta_{2}) \\ \sin(\theta_{2}) & \cos(\theta_{2}) & 0 & 200\sin(\theta_{2}) \\ 0 & 0 & 1 & 70 \\ 0 & 0 & 0 & 1 \end{bmatrix}$$

$${}^{4}_{3}T = \begin{bmatrix} \cos(\theta_{3}) & -\sin(\theta_{3}) & 0 & 0 \\ \sin(\theta_{3}) & \cos(\theta_{3}) & 0 & 0 \\ 0 & 0 & 1 & 40 \end{bmatrix}$$

$$4$$

Multiplying the derived homogeneous transformation matrices for each joint of the SCARA manipulator yields the pose transformation matrix of the end-effector frame {4} relative to the base frame $\{0\}$, expressed as [13].

$${}_{0}^{4}T = {}_{0}^{1}T {}_{1}^{2}T {}_{2}^{3}T {}_{3}^{4}T$$
 5

0
$$120 + 220\cos(\theta_1) + 200\cos(\theta_1 + \theta_2)$$

0 $220\sin(\theta_1) + 200\sin(\theta_1 + \theta_2)$
1 $z_0 + 172$
0 1

However, they incur higher computational demands and may converge to local optima. Given the elementary kinematic structure of the SCARA robot in this study, the geometric solution method is implemented, enabling efficient derivation of all joint angles.

Given specified rotational angles α , β , γ for the shoulder, elbow, and wrist joints respectively, along with prismatic joint displacement z_0 , along the z-axis, substitution into Equation (4.6) yields the resultant end-effector transformation matrix:

$$\begin{array}{cccc}
120 + 220\cos(\alpha) + 200\cos(\alpha + \beta) \\
220\sin(\alpha) + 200\sin(\alpha + \beta) \\
z_0 + 172 \\
1
\end{array}$$

$${}_{0}^{1}T^{-1} = \begin{bmatrix} 1 & 0 & 0 & -120 \\ 0 & 1 & 0 & 0 \\ 0 & 0 & 1 & -z_{0} \\ 0 & 0 & 0 & 1 \end{bmatrix}$$

Premultiplying both sides of the end-effector transformation matrix by the inverse matrix of the shoulder joint yields:

$${}^{4}T = {}^{1}_{0}T^{-1} {}^{4}_{0}T = {}^{2}_{1}T {}^{3}_{2}T {}^{4}_{3}T = \begin{bmatrix} \cos(\alpha + \beta + \gamma) & -\sin(\alpha + \beta + \gamma) & 0 & 200\cos(\alpha + \beta) + 220\cos(\alpha) \\ \sin(\alpha + \beta + \gamma) & \cos(\alpha + \beta + \gamma) & 0 & 200\sin(\alpha + \beta) + 220\sin(\alpha) \\ 0 & 0 & 1 & 172 \\ 0 & 0 & 0 & 1 \end{bmatrix}$$

8

10

 $\int_{\text{Let}}^{4} T = T_p$

$${}_{1}^{3}T = T_{p} = \begin{bmatrix} n_{x} & m_{x} & 0 & P_{x} \\ n_{y} & m_{y} & 0 & P_{y} \\ 0 & 0 & 1 & P_{z} \\ 0 & 0 & 0 & 1 \end{bmatrix}$$

Given that both matrices ${}^{0}T^{-1}, {}^{4}T$ constitute known

quantities, all elements of matrix T_p are explicitly determined, with the resulting kinematic configuration of the robotic manipulator depicted in Fig.7.

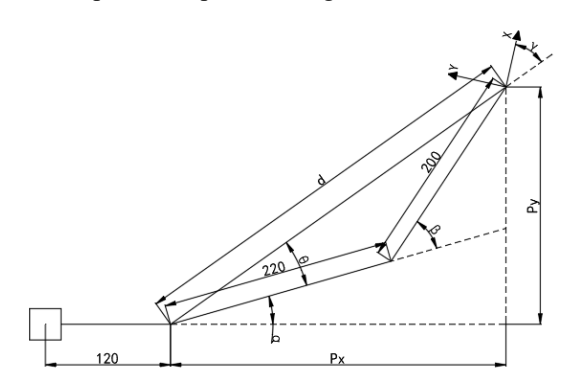


Figure .7 Inverse Kinematic Solutions

Given matrix T_p , the following equation is derived:

$$d = \sqrt{\left(p_x\right)^2 + \left(p_y\right)^2}$$
 11

$$P_x = 200\cos(\alpha + \beta) + 220\cos(\alpha)$$

$$P_{v} = 200\sin(\alpha + \beta) + 220\sin(\alpha)$$

Applying the Law of Cosines yields:

$$\cos(\pi - \beta) = \frac{L_1^2 + L_2^2 - d^2}{2L_1 L_2}$$
 14

$$\beta = \pm \arccos(\cos(\beta)) = \pm \arccos(\frac{d^2 - L_1^2 - L_2^2}{2L_1L_2})$$
 15

Applying the Law of Cosines theorem yields:

$$\cos(\theta) = \frac{d^2 + l_l^2 - l_2^2}{2dl_1^2}$$
 16

$$\theta = \pm \arccos(\cos(\theta)) = \pm \arccos(\frac{d^2 + l_1^2 - l_2^2}{2dl_1^2})$$
 17

The Py and Px coordinate values in the current frame are obtained from the elements at row 1 column 4 and row 2 column 4 of matrix T_n , respectively.

$$\tan\left(\alpha + \theta\right) = \frac{Py}{Px}$$
 18

$$\alpha = \arctan(\frac{Py}{Px}) \pm \theta$$
 19

The angular displacement between the end-effector orientation and the positive x-axis is denoted as $\alpha + \beta + \gamma$, hence the terminal rotation angle is given by

$$\gamma = \arccos(T(1,4)) - (\alpha + \beta)$$
 20

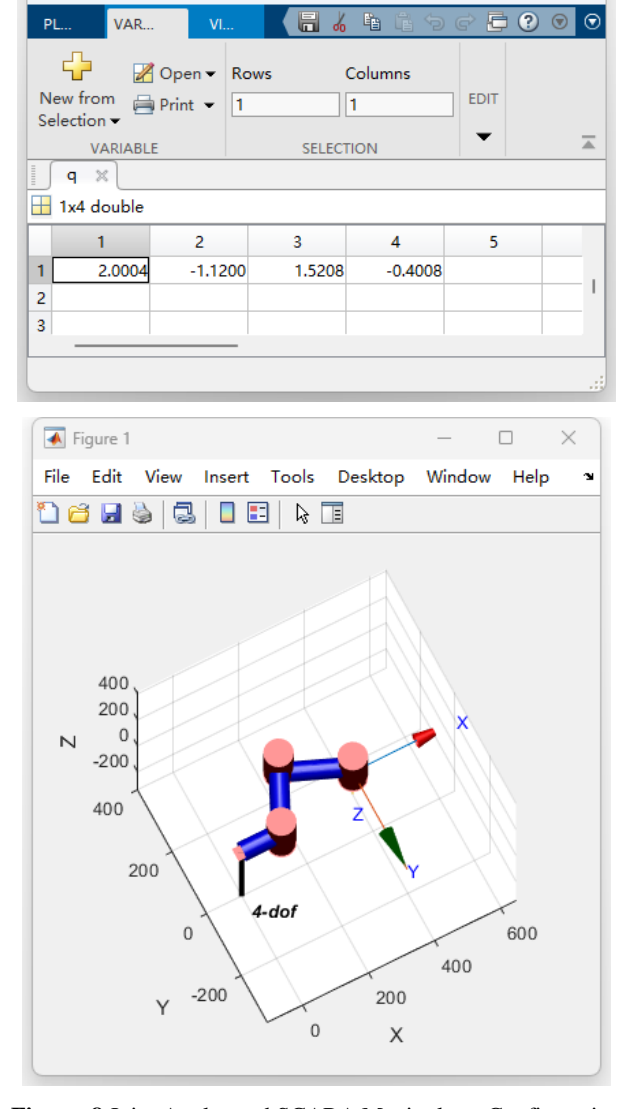
The rotational angles for each joint of the SCARA robot are given by Eqs. 4.15, 4.19, and 4.20 respectively.

To validate the correctness of the proposed inverse kinematic equations for the SCARA robot, the ikunc function in MATLAB is employed to compute joint angles for arbitrary end-effector poses. These results are compared against solutions derived from the inverse kinematic equations presented in this study, thereby verifying the accuracy of the derived analytical solutions.

When establishing a basic coordinate system in MATLAB, the basic coordinate system is in the same position as in Figure 1, but the z-axis points in the opposite direction, so the given transformation matrix is:

$$T = \begin{vmatrix} 1 & 0 & 0 & 400 \\ 0 & -1 & 0 & 120 \\ 0 & 0 & -1 & -170 \\ 0 & 0 & 0 & 1 \end{vmatrix}$$
 21

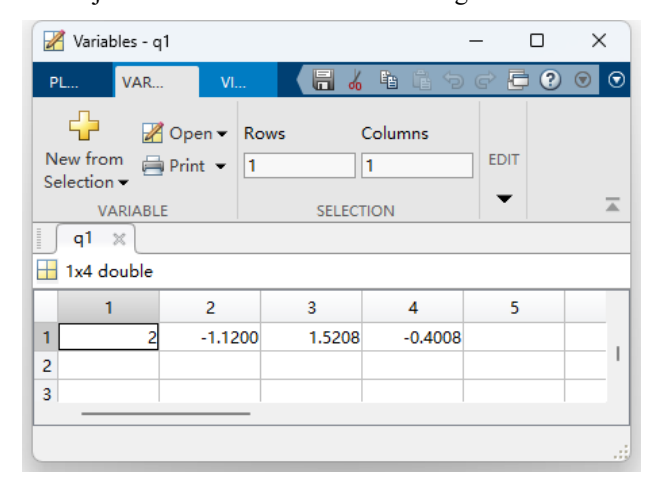
the corresponding joint motion angles are computed in MATLAB, with the resulting robot pose at these joint angles illustrated in Figure 8.



Variables - q

Figure .8 Joint Angles and SCARA Manipulator Configuration

Column 1 corresponds to the displacement of joint J0, column 2 to the rotation angle (in radians) of joint J1, column 3 to the rotation angle of joint J2, and column 4 to the rotation angle of joint J3. The previously derived equations were algorithmically implemented in MATLAB to compute translational and rotational displacements under transformation matrix (4.21), yielding two solution sets. The resultant SCARA manipulator configurations corresponding to these joint solutions are illustrated in Figures 9 and 10.



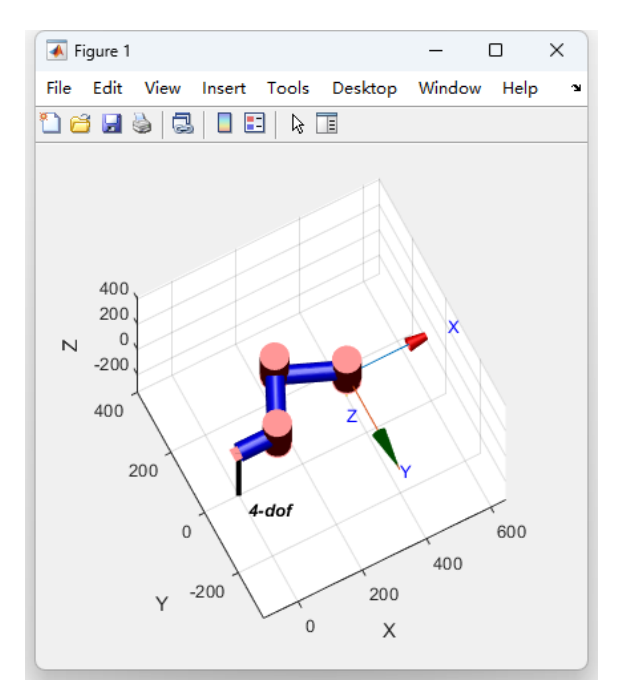
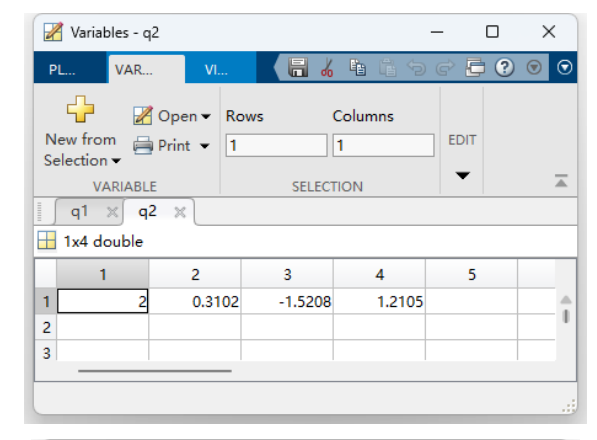


Figure .9 Primary Joint Solution and It's Kinematic Configuration



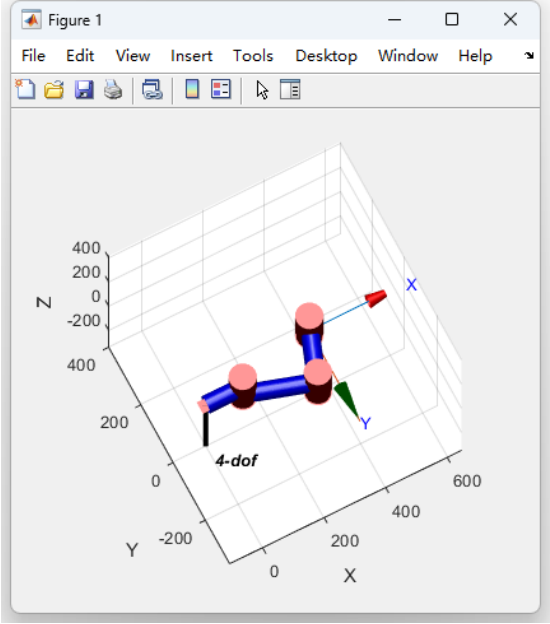


Figure .10 Secondary Joint Solution and It's Kinematic Configuration

It is demonstrated that all joint angle solutions derived from the proposed inverse kinematics equations yield consistent end-effector poses. Furthermore, the primary joint solution exhibits only minimal deviation from MATLAB's ikunc solution - specifically a marginal positional discrepancy confined to the J0 prismatic joint. These results validate the correctness of the analytical inverse kinematics formulation presented in this work.

References

- [1] Fylladitakis, E., Katemliadis, S. and Pantelaki, I. (2024) Benefits of Dielectric Oil Regeneration Systems in Power Transmission Networks: A Case Study. Journal of Power and Energy Engineering, 12, 20-29. Doi: 10.4236 / jpee. 2024. 124002.
- [2] Rigatos G, Abbaszadeh M, Busawon K, Pomares J. Nonlinear optimal control for a 4-DOF SCARA robotic manipulator. Robotica. 2023; 41(8): 2397-2450. doi: 10.1017 / S0263574723000450
- [3] Lin, J., Yang, Z., Huang, G. (2022). Motioning Planning and Vibration Suppression of Rigid-Flexible Coupled Joint SCARA Robot. In: Tan, J. (eds) Advances in Mechanical Design. ICMD 2021. Mechanisms and Machine Science, vol 111. Springer, Singapore. https://doi.org/10.1007/978-981-16-7381-8_82
- [4] Urrea, C.; Sari, P.; Kern, J. Hybrid System for Fault Tolerance in Selective Compliance Assembly Robot Arm: Integration of Differential Gears and Coordination Algorithms. Technologies 2025, 13, 47. https://doi.org/10. 3390/technologies13020047
- [5] WANG Ning. Optimized Design of SCARA Robot Large Arm based on ABAQUS Topology Optimization[J]. Mechanical Research & Application, 2023, 36(6): 8-11. DOI: 10.16576/j.ISSN.1007-4414.2023.06.003
- [6] Cao, W.A.; Li, S.; Cheng, P.; Ge, M.; Ding, H.; Lai, J. Design and development of a new 4 DOF hybrid robot with Scara motion for high-speed operations in large workspace. Mech. Mach. Theory 2024, 198, 105656.
- [7] Bouzid R, Gritli H, Narayan J. ANN approach for SCARA robot inverse kinematics solutions with diverse datasets and optimisers[J]. Applied Computer Systems, 2024, 29(1): 24-34.
- [8] Liangwen WangCA, Wenliao Du, Xiaoqi Mu, et al. A geometric approach to solving the stable workspace of quadruped bionic robot with hand-foot-integrated function[J]. Robotics and Computer-Integrated Manufacturing, 2016, Vol. 37: 68-78.

- [9] ZhiYong Yang, Wang Tian, HaoYang Wang, et al. Snake-Like Robot Workspace Solving Method Based on Improved Monte Carlo Method[J]. Applied Bionics and Biomechanics, 2025, Vol. 2025(1): 6125695.
- [10] Alnomani, Salah NooriCAa,Nassrullah,et al. Improving the workspace for a 3dof scara robot by investigating the main parameters of denavit-hartenberg approach[J]. Journal of Mechanical Engineering Research and Developments,2021,Vol.44(6): 1-8.
- [11] Guojun Xie, Huanhuan Yang, Gang ChenCA1. A framework for formal verification of robot kinematics[J]. Journal of Logical and Algebraic Methods in Programming, 2024, Vol.139: 100972.
- [12] Jun Cheng, Shaohui Hao, Ruiping Wang, et al. A method for kinematic analysis and trajectory planning of a dredging robot based on screw theory and quaternion[J]. Journal of Mechanical Science and Technology, 2025, Vol. 39(5): 2889-2900.
- [13] Yuwang Liu, Dongqi Wang, Yongchao Zhang, et al. Design and Experimental Study of Space Continuous Robots Applied to Space Non-Cooperative Target Capture[J]. Micromachines, 2021, Vol. 12(5): 536.
- [14] Minghe Jin, Liu Q, Wang B, et al. An efficient and accurate inverse kinematics for 7-dof redundant manipulators based on a hybrid of analytical and numerical method[J]. Ieee Access, 2020, 8: 16316-16330.
- [15] Zaplana I, Hadfield H, Lasenby J. Closed-form solutions for the inverse kinematics of serial robots using conformal geometric algebra[J].Mechanism and Machine Theory, 2022, 173:104835.
- [16] Rokbani N, Neji B, Slim M, et al. A multi-objective modified PSO for inverse kinematics of a 5-DOF robotic arm[J]. Applied Sciences, 2022, 12(14): 7091.
- [17] Harrade I, Daoui A, Kmich M, et al. Control of a Four Degrees of Freedom Robot Using a Sine Cosine Algorithm for Joint Position[C]. International Conference on Digital Technologies and Applications. Cham: Springer International Publishing, 2022; 791-800.
- [18] Vazquez-Santiago K, Goh C F, Shimada K. Motion planning for kinematically redundant mobile manipulators with genetic algorithm, pose interpolation, and inverse kinematics[C]. 2021 IEEE 17th International Conference on Automation Science and Engineering (CASE). IEEE, 2021: 1167-1174.